Analyzing thermo-hydrodynamics of nanofluid flowing through a wavy U-turn channel

Ashorynejad, Hamid Reza; Zarghami, Ahad; Sadeghi, Keyvan

DOI
10.1016/j.ijmecsci.2018.06.025

Publication date
2018

Document Version
Final published version

Published in
International Journal of Mechanical Sciences

Citation (APA)
Ashorynejad, H. R., Zarghami, A., & Sadeghi, K. (2018). Analyzing thermo-hydrodynamics of nanofluid flowing through a wavy U-turn channel. *International Journal of Mechanical Sciences*, *144*, 628-638. https://doi.org/10.1016/j.ijmecsci.2018.06.025

International Journal of Mechanical Sciences 144 (2018) 628–638

Contents lists available at ScienceDirect

International Journal of Mechanical Sciences

journal homepage: www.elsevier.com/locate/ijmecsci

Analyzing thermo-hydrodynamics of nanofluid flowing through a wavy U-turn channel

Hamid Reza Ashorynejad[a,*], Ahad Zarghami[b], Keyvan Sadeghi[a]

[a] Department of Industrial, Mechanical and Aerospace Engineering, Buein Zahra Technical University, Buein Zahra, Qazvin, Islamic Republic of Iran
[b] Department of Process and Energy, Delft University of Technology, Delft, The Netherlands

ARTICLE INFO

Keywords:
Wavy wall
Nanofluid
LBM
U-turn channel
Thermal–hydraulic performance factor

ABSTRACT

In this paper, the thermo-hydrodynamics of Al_2O_3-water nanofluid in a wavy U-turn channel with hot walls is numerically investigated by means of lattice Boltzmann modeling. At first, the numerical technique is validated by simulating fluid flow in a (non-)wavy straight channel. Then, the effects of various active parameters, e.g. pressure gradient in the channel, nanoparticles volume fraction, and number of sinusoidal waves along the channel, on the flow field and heat transfer is studied. Furthermore, the thermal–hydraulic performance factor is determined to investigate whether heat transfer enhancement outweighs the greater frictional losses caused by both complex wavy wall geometry and nanoparticles. The results show that the heat transfer rises by increasing pressure gradient in the channel while drops by increasing number of waves. Also, the effect of nanoparticles volume fraction on dimensionless Nusselt number becomes more pronounced at higher pressure gradients. The results indicate that the thermal–hydraulic performance factor grows by increasing nanoparticles volume fraction or decreasing the number of waves.

1. Introduction

Fluid flow with heat transfer inside channels occur in many engineering applications such as heat exchanger systems, heat sinks, cooling systems and chemical reactors [1–3]. However, the intrinsic low thermal conductivity of heat transfer fluids is considered a major drawback on the heat transfer in thermal systems. Hence, improving heat transfer rate of flows is very important for designing high efficiency engineering systems.

In recent years, nanofluids have been proposed to improve the thermal conductivity of heat transfer fluids. A nanofluid is a fluid composed of a mixture of a base fluid (such as water, organic fluids and biofluids) and a significant number of nano-scale particles (such as metals and metal oxides) and is shown to enhance heat transfer in forced convection applications [4–7]. The properties of nanofluids are dependent on physical properties of based fluid and nanoparticles, geometry and dimension of nanoparticles and existing interactions between the nanoparticles and the base fluid (such as fractions and interface effects). The precise definition of these parameters allows the precise characterization of the nanofluid. Sheikholeslami and Ganji [8] studied the effect of shape factor on nanofluid forced convection considering the impact of Lorentz forces. Their Results proved that temperature gradient augmented with rise of Darcy and Reynolds numbers while it decreased with increase of Lorentz forces.

Another distinct method to enhance heat transfer rate of fluid flows in channels is the use of complex channel geometries to induce convective transport and mixing in laminar flows [9]. The wavy walled channel is one of these complex geometries which is used widely to enhance heat transfer efficiency of industrial transport processes such as compact heat exchangers and high efficiency membrane oxygenators [9–10]. Generally, when fluid flows in wavy channels, wall corrugations create a steady vortex or swirl in laminar flows in the furrow regions of the wavy wall. The changes in flow mixing, boundary layer disruption, and thinning cause heat and mass transfer enhancement near the wavy walls.

The ability of the wavy channel geometry to enhance mixing and heat transfer has been studied extensively. A significant amount of research has been devoted, using both numerical [11–15] and experimental [16–18] techniques, to better understand the physical mechanisms behind these enhancements. The most noticeable conclusion from those investigations is that a significant increase in heat transfer is experienced when the Reynolds number increases and the flow becomes unsteady. Also, it has been demonstrated that an increase in the pressure drop always enhances the heat transfer flow in a straight channel. These conclusions indicate that using wavy walls to increase mixing is a viable option for heat transfer devices.

The usage of nanofluids in channels with wavy walls could be an effective method to enhance the rate of heat transfer in channels, significantly. Some studies have been done on nanofluid flow through wavy

* Corresponding author.
E-mail address: h.r.ashorynezhad@gmail.com (H.R. Ashorynejad).

https://doi.org/10.1016/j.ijmecsci.2018.06.025
Received 29 August 2017; Received in revised form 23 May 2018; Accepted 12 June 2018
Available online 19 June 2018

channels. Ahmed et al. [19] numerically investigated the flow and heat transfer of a copper–water nanofluid flow through a wavy channel with isothermal walls. They found that the friction coefficient and Nusselt number increase as the amplitude of wavy channel increases. In addition, it was found that the local skin-friction coefficient rises with increasing amplitude of the wavy wall for the pure water, but this augmentation is less for the case of a nanofluid. Yang et al. [20] performed an optimization procedure on the heat transfer enhancement for nanofluid flow in a two-dimensional wavy channel, for Reynolds numbers of 250–1000. They showed that the enhancement in heat transfer mainly depends on the nanoparticle volume fraction, the amplitude of wavy wall, and the Reynolds number. Heidary and Kermani [21] studied numerically heat transfer and flow field in a wavy channel with nano-fluid, and showed that the heat transfer rate inside the channel was enhanced up to 50% by using the nanoparticles and wavy walls. Akbarzadeh et al. [22] performed a sensitivity analysis by means of surface methodology in order to manage thermal and pumping power for nanofluid flow inside a wavy channel for different Reynolds numbers. They found that wavy channels with high amplitude, have a significant pressure drop which leads to an increase in pumping costs. Esfahani et al. [23] analyzed the entropy generation for the Cu-water nanofluid flow through a wavy channel. They indicated that the thermal entropy generation is main term in most part of the channel, including near the wavy walls. Moreover, they showed that the rise in viscous entropy generation with Reynolds number increases with increasing dimensionless amplitude.

In the past two decades, the lattice Boltzmann method (LBM) has attracted significant attention as an alternative technique to solve complex fluid flow problems [24–33]. The simple form of the governing equations, the space–time locality, the straightforward parallelism, the easy grid generation and the capability of incorporating complex microscopic interactions are the main advantages of the LBM. Moreover, the pressure field and the stress tensor are locally available, without the need for solving any Poisson problem [34]. The LBM is a mesoscopic method which uses the discrete Boltzmann equation to model a Newtonian fluid that is governed by the Navier–Stokes equations. As a mesoscopic method, LB method integrates both microscopic and macroscopic characteristics, which make it receive much attention in simulating nanofluid flow problems [35–36]. Kefayati and Tang [37] investigated on the natural convection and entropy generation of non-Newtonian nanofluid, using the Buongiorno's mathematical model in a cavity in the presence of a uniform magnetic field by LBM. They have shown that the increase in the Brownian motion and Thermophoresis parameters enhance the total irreversibility and ameliorate mass transfer and declines heat transfer significantly. Recently, Ashorynejad and Zarghami [38] studied the effects of uniform vertical magnetic field on thermo-hydrodynamics of nanofluids in a partially porous channel by LBM. Their results revealed that the Nusselt number is an increasing function of nanoparticle volume fraction, Hartmann number, pressure gradient and Darcy number, although the effect of Darcy numbers and pressure gradient on the temperature profile are more noticeable than others.

Fluid flow in curved channels with various bend angles has several applications in solar collectors, heat exchangers and rotary power machines such as gas turbines [39–40]. Despite the numerous studies of the force convection in wavy channels with nanofluids, to the best knowledge of the authors, there is no study on the force convection in the wavy U-turn channels with nanofluids. In the present study, the force convection heat transfer of Al_2O_3-water nanofluid in a wavy U-turn channel is simulated numerically. For this purpose, the thermal LBM with double-distribution function (DDF) model is used to capture the temperature field. The walls are assumed to be isothermal with constant high temperature. In order to carry out fundamental investigations, gain exhaustive understanding into the problem, and also examine the capability of the proposed numerical method, we first start with a two-dimensional geometry as a case study in the present work. For this purpose, the effect of various physical parameters, such as volume fraction of nanoparticles, pressure gradient in channel, and geometry of wavy walls on heat transfer rate are investigated. The results of this study can be used at design decisions by engineers for the aforementioned applications.

The rest of the paper are structured as follows: Section 2 presents the thermal LBM for simulating nanofluids. In Section 3 the flow and temperature boundary conditions for lattice Boltzmann modeling are presented, comprehensively. The numerical results are presented in Section 4. Finally, the concluding remarks are given in Section 5.

2. Thermal LBM for nanofluids

2.1. LBM for fluid flow

The general lattice Boltzmann equation with the BGK approximation for simulating single-phase flow is derived as following [34]:

$$\frac{f_i\left(\vec{x}+\vec{e}_i\Delta t, t+\Delta t\right)-f_i\left(\vec{x},t\right)}{\Delta t}=-\frac{1}{\tau}\left(f_i(\vec{x},t)-f_i^{eq}\left(\vec{x},t\right)\right) \tag{1}$$

where $\vec{x}$ is spatial coordinate, t is time, $f_i(\vec{x},t)$ is the density distribution function associated with discrete velocity direction i and τ is the relaxation time. The discrete velocities $\vec{e}_i$ in the ith-direction, for the D_2Q_9 lattice are given by $\vec{e}_0=0$ and $\vec{e}_i=\lambda_i(\cos\theta_i,\sin\theta_i)$ with $\lambda_i=1,\theta_i=(i-1)\pi/2$ for $i=1\sim 4$and $\lambda_i=\sqrt{2},\theta_i=(i-5)\pi/2+\pi/4$ for $i=5\sim 8$. The order number $i=1\sim 4$ and $i=5\sim 8$ represent the rectangular and the diagonal directions of the lattice, respectively. Also, f_i^{eq} is the equilibrium distribution function and is calculated as:

$$f_i^{eq}=w_i\rho\left[1+\frac{\left(\vec{e}_i\cdot\vec{u}\right)}{c_s^2}+\frac{\left(\vec{e}_i\cdot\vec{u}\right)^2}{2c_s^4}-\frac{\left(\vec{u}\cdot\vec{u}\right)}{2c_s^2}\right] \tag{2}$$

where $c_s=1/\sqrt{3}$ is the lattice speed of sound, and w_i are the weighting factors, equal to 4/9 for $i=0$, 1/9 for $i=1\sim 4$ and 1/36 for $i=5\sim 8$. The local mass density, the local velocity and the viscosity in the lattice units are calculated as $\rho=\sum_i f_i$, $\vec{u}=(\sum_i \vec{e}_i f_i)/\rho$ and $\nu=(\tau-0.5)/3$, respectively. Eq. (1) is usually solved through the standard collision and streaming steps as:

$$\text{Collision}: \tilde{f}_i\left(\vec{x},t+\Delta t\right)=f_i\left(\vec{x},t\right)-\frac{\Delta t}{\tau}\left(f_i\left(\vec{x},t\right)-f_i^{eq}\left(\vec{x},t\right)\right) \tag{3}$$

$$\text{Streaming}: f_i\left(\vec{x}+\vec{e}_i\Delta t,t+\Delta t\right)=\tilde{f}_i\left(\vec{x},t+\Delta t\right) \tag{4}$$

where $\tilde{f}_i$ represents the post-collision state. The simulation is performed on a structured Cartesian grid where unit spacing is utilized the dimensionless lattice units, i.e. $\Delta x=\Delta t=1$. During the streaming step the particles move from one node to its neighbor node, according to the set of discrete velocities. Computationally speaking, during the streaming step all distribution functions are copied to the adjacent cell in the direction of the lattice vector. Therefore, the streaming step involves very little computational effort. On the other hand, during the collision step the particles relax towards local equilibrium according to the BGK operator [34,41].

2.2. Thermal LBM

Ignoring viscous heat dissipation, the thermal LBM based on the double distribution function (DDF) model is expressed as follows [42]:

$$\frac{g_i\left(\vec{x}+\vec{e}_i\Delta t,t+\Delta t\right)-g_i\left(\vec{x},t\right)}{\Delta t}=-\frac{1}{\tau_g}\left(g_i-g_i^{eq}\right) \tag{5}$$

where the g_i's denote the energy distribution functions, τ_g is the thermal relaxation time and g^{eq} denotes the energy equilibrium distribution functions given by:

$$g_i^{eq}=w_iT\left[1+\frac{\left(\vec{e}_i\cdot\vec{u}\right)}{c_s^2}+\frac{\left(\vec{e}_i\cdot\vec{u}\right)^2}{2c_s^4}-\frac{\left(\vec{u}\cdot\vec{u}\right)}{2c_s^2}\right] \tag{6}$$

Table. 1
Thermophysical properties of nanoparticles at 30 °C [50].

Property	Al_2O_3
c_p (J/KgK)	765
ρ (Kg/m^3)	3970
k (W/mK)	25
d (nm)	47

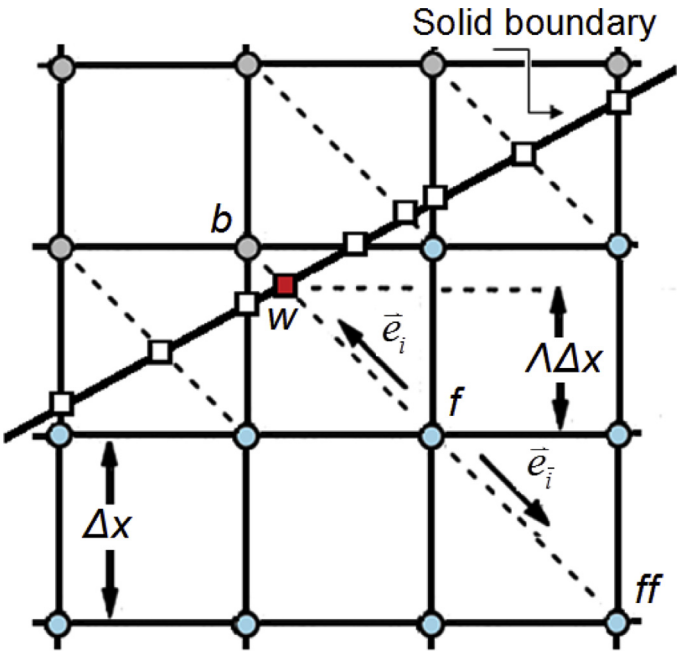

Fig. 1. Sketch of the bounce back boundary condition scheme for an arbitrary shaped solid wall.

Table. 2
Results from grid independence test for a U-turn channel with four waves, $P_0 = 30$ and $\phi = 0$.

Mesh size	Nu_{ave}	%Change	Re	%Change
200 × 80	8.182	1.44%	108.60	0.96%
250 × 100	8.242	0.72%	109.01	0.59%
300 × 120	8.301	0.04%	109.66	0.03%
400 × 160	8.304	–	109.71	–

where $T = \sum_i g_i$ is the temperature and $\alpha = (\tau_g - 0.5)/3$ is the thermal diffusivity. It is worth mentioning that the DDF approach is based on the principle that the isothermal LBM can be directly derived by properly discretizing the continuous Boltzmann equation in temporal, spatial, and velocity spaces. This model assumes that the viscous dissipation and compression work can be neglected for incompressible fluids and the evolution of the temperature is given by the advection–diffusion equation. Hence, the temperature is considered as a passive scalar transported by the speed without changing the velocity field [43,44].

2.3. Thermo-physics of nanofluids

To develop the LBM for nanofluid, mesoscopic properties should be changed due to interaction between nanoparticle and base fluid. Both the base fluid and the nanoparticles are assumed to be in thermal equilibrium and to move with the same local velocity. The properties of water and Alomina nanoparticles are listed in Table 1. The density (ρ), and specific heat (C_p) of nanofluid are obtained from the following formula [45]:

$$\rho_{nf} = (1-\phi)\rho_f + \phi\rho_{np} \tag{7}$$

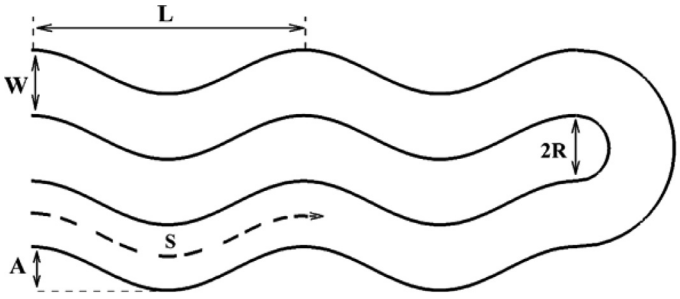

Fig. 2. Schematic of simulation domain with $n = 4$.

$$(\rho C_p)_{nf} = (1-\phi)(\rho C_p)_f + \phi(\rho C_p)_{np} \tag{8}$$

where φ is the volume fraction of the nanoparticles and subscripts *f*, *nf* and *np* denote the base fluid, nanofluid and solid nanoparticles, respectively. The Effective viscosity of nanofluid, μ_{nf}, is calculated as a function of temperature and the volume fraction of nanoparticles with the following correlation was presented by Abu-Nada [46]:

$$\mu_{nf} = -0.155 - \frac{19.582}{T} + 0.794\phi + \frac{2094.47}{T^2} - 0.192\phi^2 - 8.11\frac{\phi}{T} - \frac{27463.863}{T^3} + 0.0127\phi^3 + 1.6044\frac{\phi^2}{T} + 2.1754\frac{\phi}{T^2} \tag{9}$$

where the viscosity and temperature are expressed in centi poise and centigrade. It is clear that the effective viscosity increases (decreases) by increasing the particle volume fraction (temperature). The effective thermal conductivity of the nanofluid, k_{nf}, is approximated by [47]:

$$k_{nf} = k_f + k_p\left(\frac{A_p}{A_f}\right) + ck_pP_e\left(\frac{A_p}{A_f}\right) \tag{10}$$

where c is constant and evaluated experimentally, $P_e = u_p d_p/\alpha$, and

$$A_p/A_f = \frac{d_p}{d_f}\frac{\phi}{1-\phi} \tag{11}$$

where d_p is the diameter of solid particles and d_f is the diameter of liquid particles (see Table 1). Also, u_p is the Browning motion velocity which is calculated as:

$$u_p = \frac{2TK_B}{\pi d_p^2 \mu_f} \tag{12}$$

For more accurate simulation in this study, some properties of the base fluid (i.e. water) are allowed to vary with temperature. The expressions of temperature dependent thermo-physical properties are given as follows [48–50]:

$$\rho(T) = 1000\left[1 - \frac{(T+15.9414)}{508929.2(T-204.87037)}(T-276.9863)^2\right] \tag{13}$$

$$\mu(T) = 1.005\times10^{-3}\left(\frac{T}{293}\right)^{8.9}\exp\left[4700\left(\frac{1}{T}-\frac{1}{293}\right)\right] \tag{14}$$

$$C_P(T) = 3908 + 3.826T - 0.01674T^2 + 2.33\times10^{-5}T^3 \tag{15}$$

$$k_f(T) = -1.579 + 0.01544T - 3.515\times10^{-5}T^2 + 2.678\times10^{-8}T^3 \tag{16}$$

3. Boundary conditions

3.1. Flow inlet/outlet boundary condition

The nanofluid flow is driven in the channel by a constant pressure gradient, i.e. $P_{inlet} = P_{atm} + p_x$ and $P_{outlet} = P_{atm}$, where p_x represents a constant pressure gradient. In order to apply the boundary condition

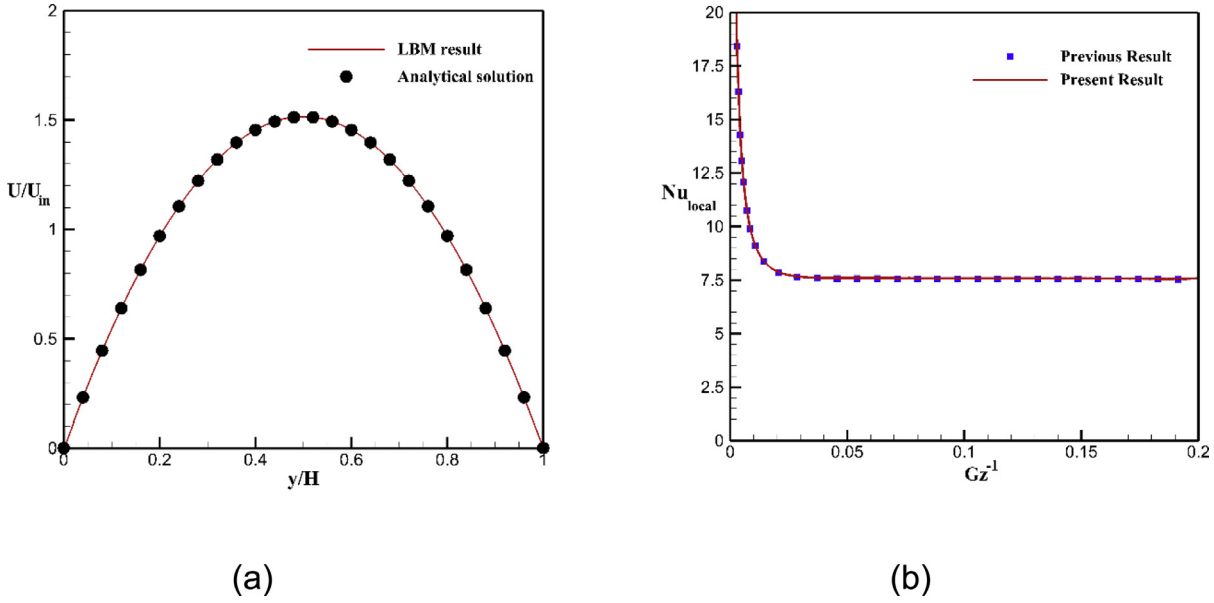

Fig. 3. Comparison of (a) velocity profile and (b) local Nusselt number distribution in a channel for present study and previous studies [50].

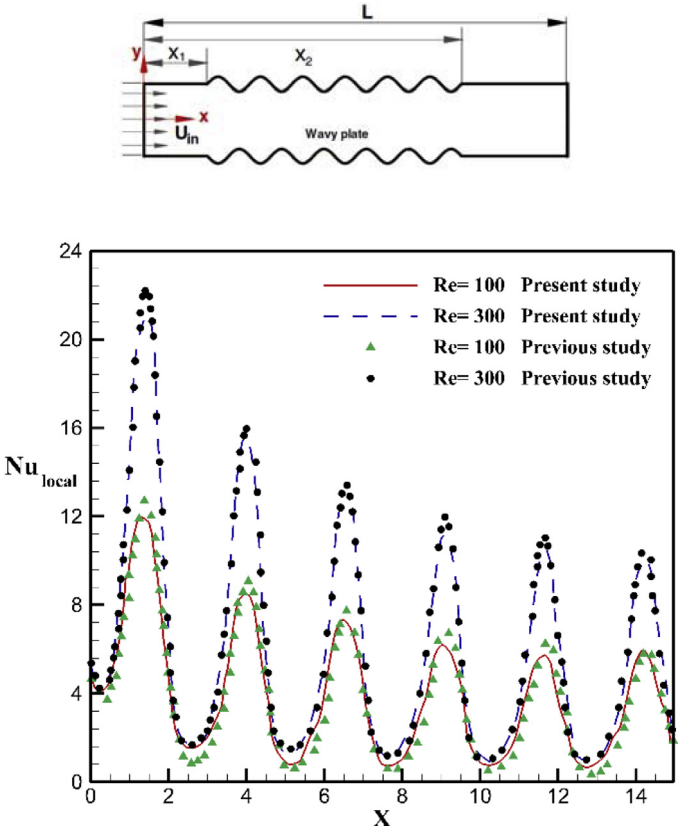

Fig. 4. Comparison between the numerical solution and previous study [60] for local Nusselt number distribution along wavy wall with constant temperature at two different Re numbers and Pr = 6.93.

with a constant pressure gradient in the LBM, the so-called Zuo–He scheme [51] is implemented. The unknown distribution functions at inlet (here: f_1, f_5 and f_8) are determined as:

$$u_{in} = 1 - \left[f_0 + f_2 + f_4 + 2\left(f_3 + f_6 + f_7\right)\right] \tag{17}$$

$$f_1 = f_3 + \frac{2}{3\rho_{in}u_{in}} \tag{18}$$

$$f_5 = f_7 + \frac{1}{2}\left(f_4 - f_2\right) + \frac{1}{6\rho_{in}u_{in}} \tag{19}$$

$$f_8 = f_6 + \frac{1}{2}\left(f_2 - f_4\right) + \frac{1}{6\rho_{in}u_{in}} \tag{20}$$

where $\rho_{in} = \rho + 72P_0\rho\nu^2 S/W^3$, W is the channel height, S is the length of the channel centerline (see Fig. 2) and P_0 represents a dimensionless pressure gradient in the lattice units [38,52]. Since, the density and viscosity in this simulation are affected by temperature, the average density and viscosity throughout the channel are used in the above equation for calculating the inlet density. A similar equations are written for the unknown distribution functions at outlet with $\rho_{out} = \rho$.

3.2. No-slip boundary condition for curved walls

In order to model the wavy walls as no-slip boundaries in the LBM, the enhanced bounce-back procedure proposed by Mei et al. [53,54] is applied. Fig. 1 depicts the schematic of the wall boundary condition for an arbitrary shaped moving object between the lattice nodes of spacing Δx. In this figure, b and f denote the lattice nodes on the solid and fluid side, respectively, and w denotes the intersections of the wall with the particle velocity directions. The corresponding solid, fluid and wall positions are given by $\vec{x}_b$, $\vec{x}_f$ and $\vec{x}_w$, and the distance between the solid node and the wall node can be calculated as $\Lambda \bullet \Delta x$, where $\Lambda = |x_f - x_w|/|x_f - x_b|$. Subscript i denotes the direction from a fluid node to a wall node along a particle velocity direction and subscript $\bar{i}$ denotes the reverse direction, i.e., from a fluid node to a wall node. Therefore, $\vec{e}_{\bar{i}} = -\vec{e}_i$ defines the velocity of particles moving along the ith direction from x_b to x_f.

After the collision step, the probability density function on the solid side (i.e. $\tilde{f}_{\bar{i}}(\vec{x}_b, t)$) is unknown and is recovered by using the following interpolation scheme [55]:

$$\tilde{f}_{\bar{i}}\left(\vec{x}_b, t\right) = (1-\chi)\tilde{f}_i\left(\vec{x}_f, t\right) + \chi f_i^*\left(\vec{x}_b, t\right) \tag{21}$$

where

$$f_i^*\left(\vec{x}_b, t\right) = w_i\rho\left(\vec{x}_f, t\right)\left[1 + \frac{\left(\vec{e}_i \cdot \vec{u}_{bf}\right)}{c_s^2} + \frac{\left(\vec{e}_i \cdot \vec{u}_f\right)^2}{2c_s^4} - \frac{\left(\vec{u}_f \cdot \vec{u}_f\right)}{2c_s^2}\right] \tag{22}$$

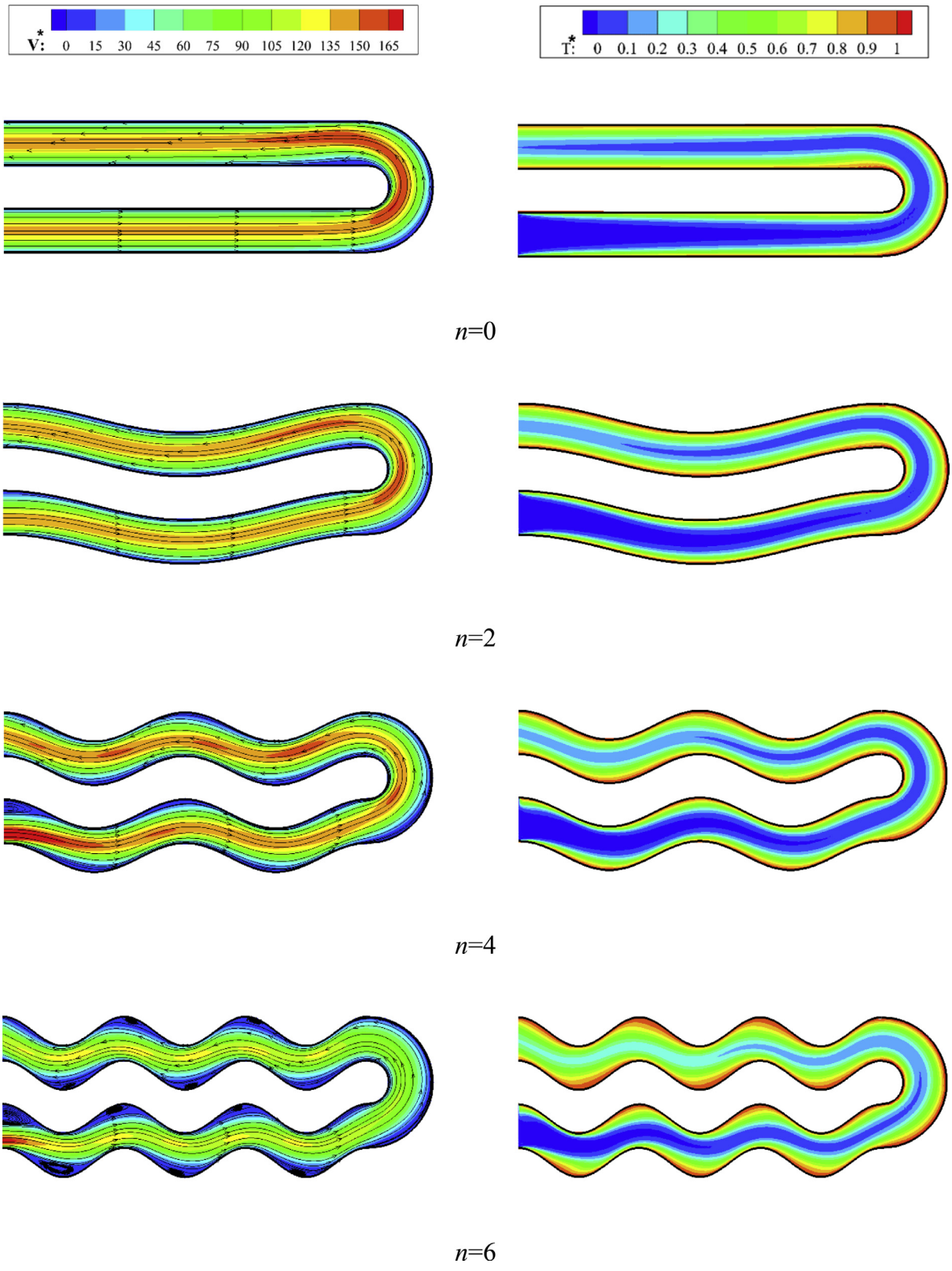

Fig. 5. Velocity magnitude and stream lines (left panels) and temperature contours (right panels) in a U-turn channel with various number of waves ($n = 0, 2, 4, 6$) for $P_0 = 50$, and $\varphi = 0$.

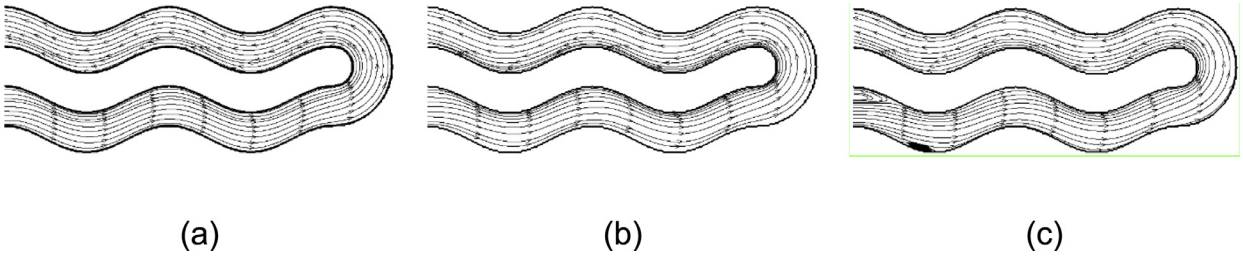

Fig. 6. Streamlines in a U-turn wavy channel with $n=4$ and $\varphi=0.02$ for (a) $P_0=10$, (b) $P_0=30$ and (c) $P_0=50$.

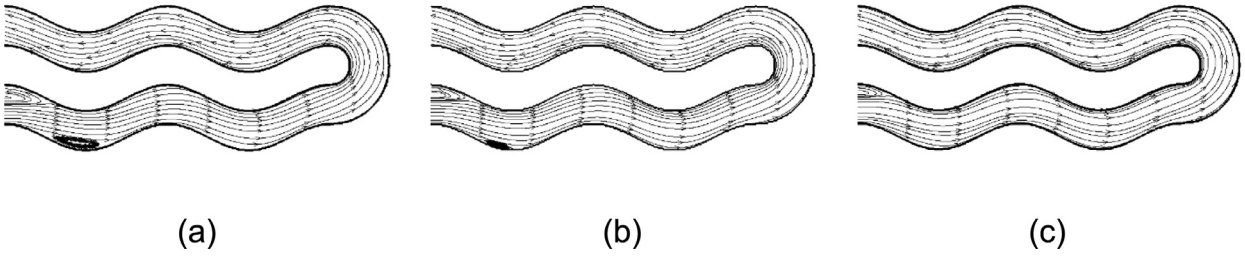

Fig. 7. Streamlines in a U-turn wavy channel with $n=4$ and $P_0=50$ for (a) $\varphi=0$, (b) $\varphi=0.02$ and (c) $\varphi=0.03$.

and $\chi=(2\Lambda-1)/(\tau-2)$and $u_{bf}=u_{ff}$ if $\Lambda<0.5$, and $\chi=(2\Lambda-1)/(\tau+0.5)$and $u_{bf}=[(\Lambda-1)/\Lambda]u_f$ if $0.5\leq\Lambda<1$. This scheme formulates a fictitious distribution function at the solid nodes and then executes the collision step at those nodes. Substantial evidence shows that the bounce-back boundary conditions combined with interpolation schemes, and including the one-half grid spacing correction at boundaries, are second-order accurate and thus capable of handling curved boundaries quite well [53–55].

3.3. Thermal inlet/outlet boundary condition

The channel inlet is kept at a constant temperature T_{in}, so the unknown distributions functions are calculated on the left boundary by [56]:

$$\begin{aligned} g_1 &= T_{in}(w_1+w_3)-g_3 \\ g_5 &= T_{in}(w_5+w_7)-g_7 \\ g_8 &= T_{in}(w_8+w_6)-g_6 \end{aligned} \tag{23}$$

For the outflow, the convective boundary condition is applied. This condition can be written as:

$$\frac{\partial T}{\partial x}+\vec{U}\frac{\partial T}{\partial x}=0 \tag{24}$$

where $\vec{U}=\vec{u}(N-1,j,t)$ is a typical velocity normal to the outlet boundary [57]. The mesoscopic representative of the convective boundary condition for the unknown distribution functions at outlet boundary located at $x=N$ is expressed as follows [57]:

$$g_i(N,j,t+1)=\frac{g_i(N,j,t)+\lambda g_i(N-1,j,t+1)}{1+\lambda} \tag{25}$$

where $\lambda=U(t+1)$, which is known after the streaming step at the $(N-1)$th layer.

3.4. Constant temperature for curved walls

It is assumed that the channel wavy walls are in constant temperature T_{wall}. Following the method presented by Guo et al [58], the distribution function at a wall node which has a link across the physical boundary is decomposed into its equilibrium and nonequilibrium parts as follows:

$$\tilde{g}_{\bar{i}}(x_w,t)=g_{\bar{i}}^{eq}(x_w,t)+\left(1-\tau_g^{-1}\right)g_{\bar{i}}^{neq}(x_w,t) \tag{26}$$

Here, $g_{\bar{i}}$ represents the unknown distribution functions coming from the solid node into the fluid region (see Fig. 1). The equilibrium part is then approximated with a fictitious one where the boundary condition is enforced, and the nonequilibrium part is approximated using a first-order extrapolation based on the nonequilibrium part of the distribution on the neighboring fluid node.

$$g_{\bar{i}}^{eq}(x_w,t)=w_{\bar{i}}T_b^*\left[1+3\left(\vec{e}_{\bar{i}}\cdot u_b^*\right)\right] \tag{27}$$

$$g_{\bar{i}}^{neq}(x_w,t)=\Lambda g_{\bar{i}}^{neq}(x_f,t)+(1-\Lambda)g_{\bar{i}}^{neq}(x_{ff},t) \tag{28}$$

where for $\Lambda>0.75$:

$$\begin{cases} T_b^*=\dfrac{1}{\Lambda}\left[T_w+(\Lambda-1)T_f\right] \\ u_b^*=\dfrac{1}{\Lambda}\left[u_w+(\Lambda-1)u_f\right] \end{cases} \tag{29}$$

and for $\Lambda\leq0.75$:

$$\begin{cases} T_b^*=\dfrac{1}{\Lambda}\left[T_w+(\Lambda-1)T_f\right]+\dfrac{1-\Lambda}{1+\Lambda}\left[2T_w+(\Lambda-1)T_{ff}\right] \\ u_b^*=\dfrac{1}{\Lambda}\left[u_w+(\Lambda-1)u_f\right]+\dfrac{1-\Lambda}{1+\Lambda}\left[2u_w+(\Lambda-1)u_{ff}\right] \end{cases} \tag{30}$$

The heat transfer rate in the channel is characterized using local, average and mean Nusselt numbers as:

$$Nu_{local}=-\frac{k_{nf}}{k_f}\frac{D_h}{T_w-T_m(s)}\frac{\partial T}{\partial n} \tag{31}$$

$$Nu_{ave}=\frac{1}{2}\left(Nu_{local,top}+Nu_{local,bottom}\right) \tag{32}$$

$$Nu_{mean}=\frac{1}{s}\int_0^S Nu_{ave}ds \tag{33}$$

Here D_h and $T_m(s)$ are the hydraulic diameter (here: equal to $2W$) and bulk mean temperature along the channel defined as:

$$T_m(s)=\frac{\int_y T(x,y)U(x,y)dy}{\int_y U(x,y)dy} \tag{34}$$

The thermal–hydraulic performance factor is an important parameter in the heat exchangers to indicate interaction of pressure drop and

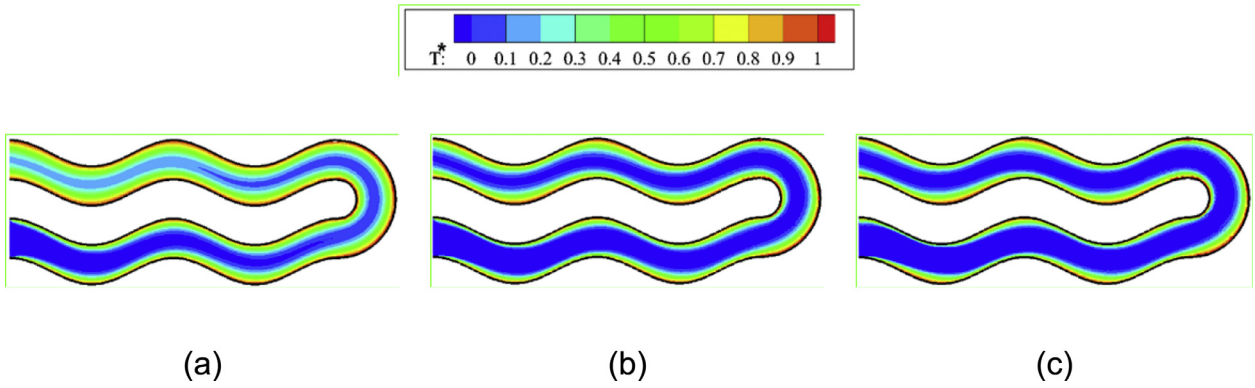

Fig. 8. Temperature contours in a U-turn wavy channel with $n=4$ and $\varphi=0.03$ for (a) $P_0=10$, (b) $P_0=30$ and (c) $P_0=50$.

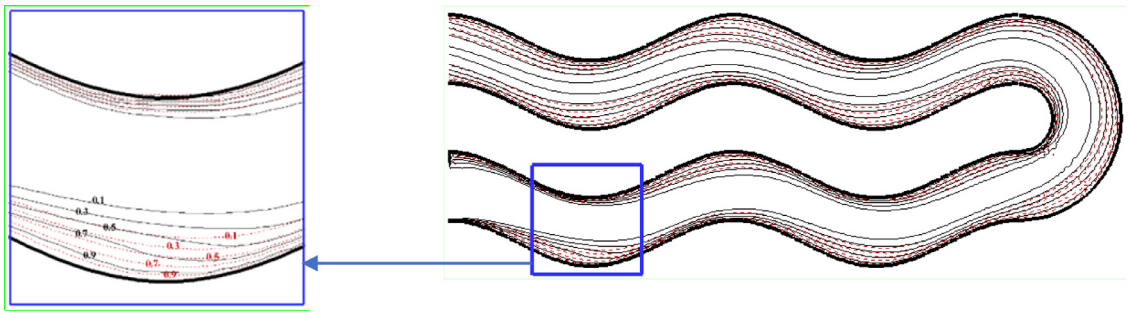

Fig. 9. Comparisons of dimensionless isotherm contours for the pure fluid (solid lines) and Nano-fluid with $\varphi=3\%$ (dashed lines) for $P_0=50$.

heat transfer and it is defined by [59]:

$$\eta=\frac{Nu/Nu_0}{\left(f/f_0\right)^{1/3}} \tag{35}$$

where, $f=(2p_xD_h)/(\rho\vec{u}^2)$ is the channel friction factor. The parameters f_0 and Nu_0 in above equation are the reference friction factor and reference Nusselt number on the flat U-turn channel without nano particles. The velocity $\vec{u}$ in this equation relates to mean velocity at the middle of channel. The dimensionless temperature and velocity are defined as:

$$T^*=\frac{T-T_{in}}{T_w-T_{in}} \tag{36}$$

$$u^*=\frac{uD_h}{\nu}\quad,\quad v^*=\frac{vD_h}{\nu}\quad,\quad V^*=\sqrt{(u^*)^2+(v^*)^2} \tag{37}$$

4. Results and discussions

4.1. Problem statement

A schematic diagram of wavy U-turn channel is shown in Fig. 2, where Al_2O_3-water nanofluid flows through it due to the constant pressure gradient. The upper and lower walls are separated by a distance W, and the periodic shape of both walls is described by $f(x)=A\sin(2\pi nx/L)$, where A, L and n are the amplitude, the length and the period of the wall oscillations, respectively. The centerline of the channel, S, is shown by dashed lines in Fig. 2. The normalized amplitude $A^*=A/W=0.33$ and $L=8.33\,W$ are used for all simulations, while number of waves (or periods) along the U-turn channel are set to $n=2$, 4 and 6. The nanofluid is supposed to be laminar, steady and incompressible and enters as a coolant to the domain with constant temperature $T_{in}=293$ K. Also, the wavy walls are kept at constant hot temperature $T_{wall}=313$ K. Calculations are performed for different values of the volume fraction (i.e. $\varphi=0\%$, 2% and 3%) and dimensionless pressure gradient ($P_0=10$, 30 and 50). Also, the Reynolds number is defined as $\mathrm{Re}=u_mD_h/\nu$, where u_m is the mean velocity of the flow and $D_h=2\,W$ is the hydraulic diameter.

4.2. Validation

The presented numerical technique is validated by reproducing solutions for some benchmark problems. At first, the fluid flow and forced convection heat transfer in a parallel-plate channel subjected to constant wall temperature is simulated. As expected from classic results for this problem, the flow will be developing in the entrance region until it reaches fully developed condition, where no further changes in velocity profile take place in the streamwise direction. Since the pressure gradient in the fully developed region is constant, the velocity profile is parabolic, with the maximum velocity at the centerline and equal to 1.5 times the mean velocity. The streamwise velocity profile in the fully developed region calculated by the LBM is shown in Fig. 3(a). A perfect agreement is observed between the numerical result and the analytical solution. The local Nusselt number calculated by the LBM shows only 0.12% deviation from the $\mathrm{Nu}_{local}=7.54$ mentioned by many authors such as ref. [50].

Now, the method is validated against previously published results of Wang and Chen [60] for force convection in a straight wavy-wall channel with $\mathrm{Pr}=6.93$ and $Re=100$ and 300. They calculated the local Nusselt number along the wavy surface. The results are shown in Fig. 4 and a good agreement is observed between the models. Fig. 4 shows that Nu_{local} is higher in the converging section of each wave than in the diverging section. The reason is that the flow has a higher average velocity and velocity gradient in the converging sections, which increases the heat transfer rate. Conversely, the minimum values of the Nu appear near the maximum cross-sections. This is due to a decrease in the convective heat transfer effect with the velocity. Also, it can be seen that Nu_{local} has a maximum value in the first wave, and it has the same tendency after the tertiary wave. This is because the thermal boundary layers are formed. Furthermore, as the Reynolds number increases, Nu_{local} along the wavy wall will also increases.

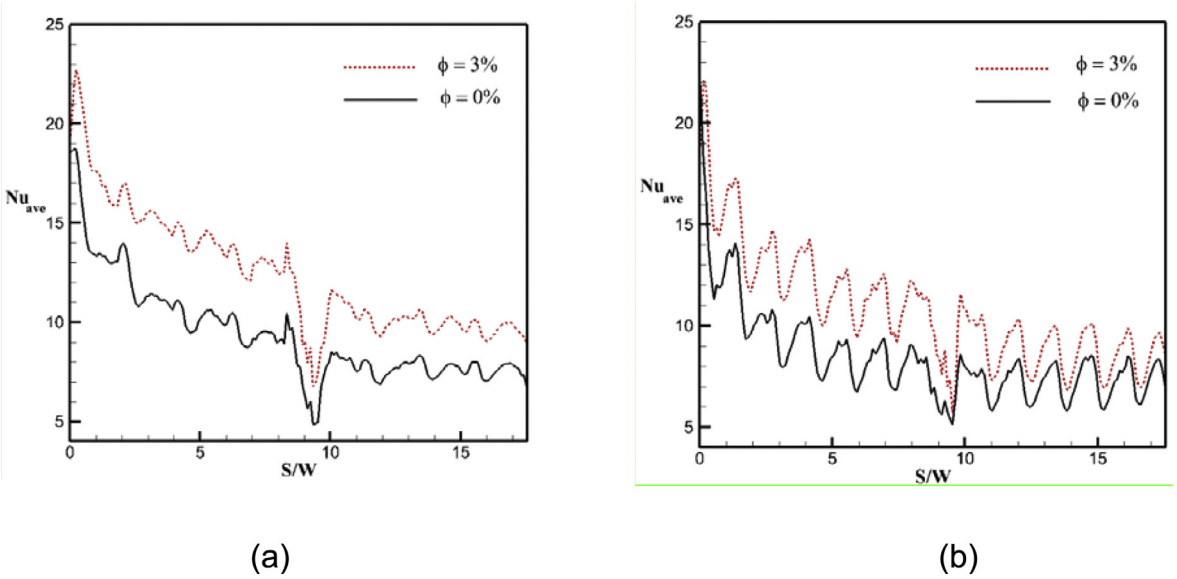

Fig. 10. Averaged Nusselt number along the channel for pure fluid (i.e. $\varphi = 0$) and nanofluid with $\varphi = 0.03$ at $P_0 = 50$ for a channel with (a) $n = 4$ and (b) $n = 6$ waves channel.

4.3. Mesh dependency test

At first, a grid refinement study is performed in order to assess the accuracy of the results and to determine the necessary grid spacing for our investigation. Table 2 gives a summary of the grid independence tests for a U-turn wavy channel with four waves, $P_0 = 30$, $\varphi = 0$. Table 2 contains the values of Nu_{ave} and Re calculated for each grid resolution along with their percent differences from the values obtained for the highest selected resolution (i.e. 400×160). Note that the following convergence criterion, ε, is used in the present study for the termination of all computations:

$$\varepsilon = \frac{\sum_{i=1}^{N}\sum_{j=1}^{M}\left|T^{n+1} - T^{n}\right|}{\sum_{i=1}^{N}\sum_{j=1}^{M}\left|T^{n}\right|} \tag{38}$$

where, n, N and M represent iteration number and the number of grid points in x and y directions, respectively. It can be seen in Table 2 that the values of N_{ave} and Re obtained using 300×120 nodes differ from those obtained using 400×160 by only 0.04% and 0.03%, respectively. Because the grid with 300×120 nodes provides nearly identical results with those of highest resolution at significantly lower computational costs, we used this grid size in our simulations.

4.4. Flow in a wavy U-turn channel

Streamlines and temperature contours for a wavy U-turn channel with $P_0 = 50$ and $\varphi = 0$ for a range of n (number of waves) from $n = 0$ (flat channel) to $n = 6$ are shown in Fig. 5. Generally for $n = 0$, the flow at the inlet section is similar to the flow between two parallel flat plates and axial symmetry is obvious. When the flow reaches the curve, this symmetry becomes concealed and the bulk flow tends to move to the inner wall. At the end of the curve, the flow separates from inner wall and the reversed flow occurs near the inner wall of outlet section; if the curvature radius is large enough there will not be any separation.

In terms of hydrodynamics (see Fig. 5, left panels), by increasing the number of waves in a constant length of the U-turn channel, the adverse pressure gradient in the cavity portions of the waves becomes pronounced and as a result, lateral vortices are created in trough (crest) of lower (upper) wall. The wall waviness creates changes in the heat transfer rate (see Fig. 5, right panels). By increasing the number of waves, better mixing occurs in the cavity regions that in turn increases the rate of heat transfer.

Fig. 6 shows the velocity streamlines for Al_2O_3-water nanofluid in a wavy channel with $n = 4$ and $\varphi = 0.02$ for different pressure gradients, P_0. Generally by increasing the pressure gradient, the Re number in the channel increases as $Re \approx 38$, 110 and 212 corresponding to $P_0 = 10$, 30 and 50, respectively. When the fluid enters to each wave, its motion is affected by two major influences. The expansion of the channel cross-section and the resulting deceleration of the fluid motion that causes an adverse pressure gradient and opposes the fluid flow. At low Re numbers (see Fig. 2(a)), the inertia of the flow is small and streamlines largely follow the wall shape due to the large viscous effect, and no recirculation region is formed in the furrow regions. As the Re number increases, a recirculating region appears in the upstream part of the furrow. By further increasing the Re number, the backflow becomes more intense and the center of the recirculating cell shifts downstream. The recirculation region is the major key feature of the fluid flow in a wavy channel [27]. Compared to the flow in a flat channel, this feature results in streamline curvature and non-zero wall-normal velocity in the wavy channel. These non-zero wall-normal mean velocities and their non-negligible spatial gradient play a significant role in flow mixing and heat transfer that is not possible in a channel flow with flat walls. The effect of nanoparticle volume fraction on the flow streamlines is shown in Fig. 7. By increasing the nanoparticle concentration, the viscosity increases (see Eq. (9)), which indicates that the overall Re number decreases. Hence, by increasing the nanoparticle volume fraction, the recirculation regions formed in the trough of the wavy wall are damped.

Fig. 8 shows the temperature distribution inside a wavy channel with $n = 4$ and $\varphi = 0.03$ for $P_0 = 10$, 30 and 50. For $P_0 = 10$, the streamlines closely follow the channel shape (see Fig. 6a) which leads to the cooling fluid located in the center of the channel remaining near the center of the channel and away from the hot walls, resulting in a minor increase in Nu_{mean} compared to the flat channel. By increasing P_0, the flow rate increases and the reversal flow occurs in trough (crest) of lower (upper) wall. By further increasing P_0, the size of recirculation regions increases and hence the strength of these recirculation regions to the main flow is pronounced, therefore the flow becomes more disturbed. Furthermore, the core fluid must turn to pass through the channel [61], and interacts more with the recirculation regions. This mechanism can improve the fluid mixing in core with that near the walls. Also it should be mentioned that by increasing the Re number, the thickness of thermal boundary layer decreases and the temperature gradient at the upper and lower walls of wavy channel increases due to the improvement of the mixing

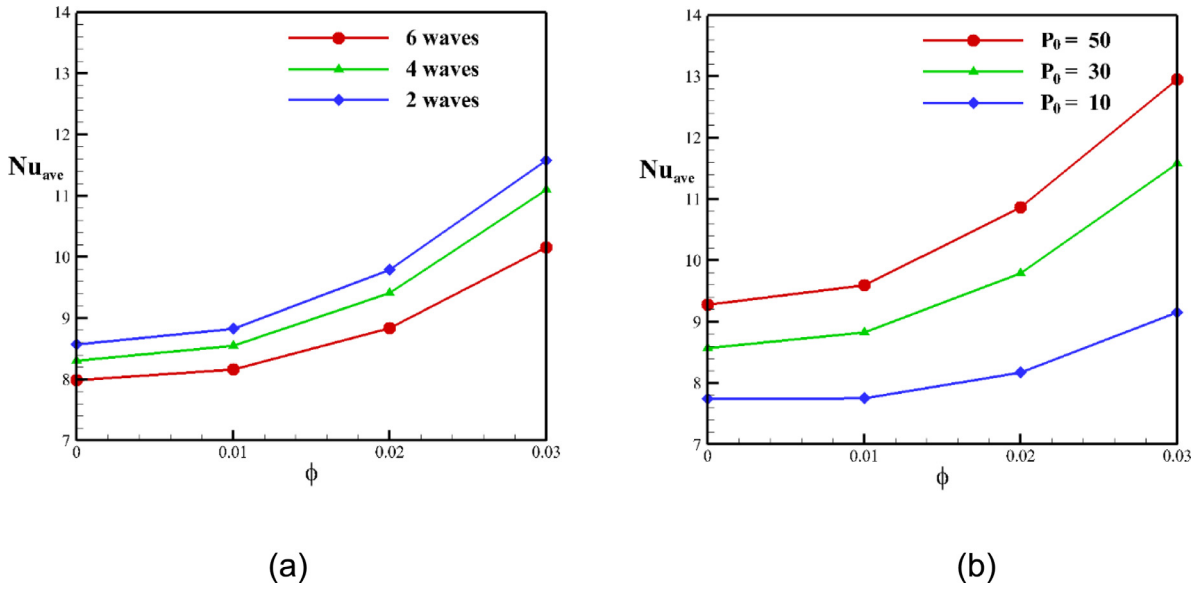

Fig. 11. Averaged Nusselt number for wavy U-turn channel as a function of nanoparticle volume fraction with (a) various number of waves for $P_0 = 30$ and (b) different pressure gradients at $n = 2$.

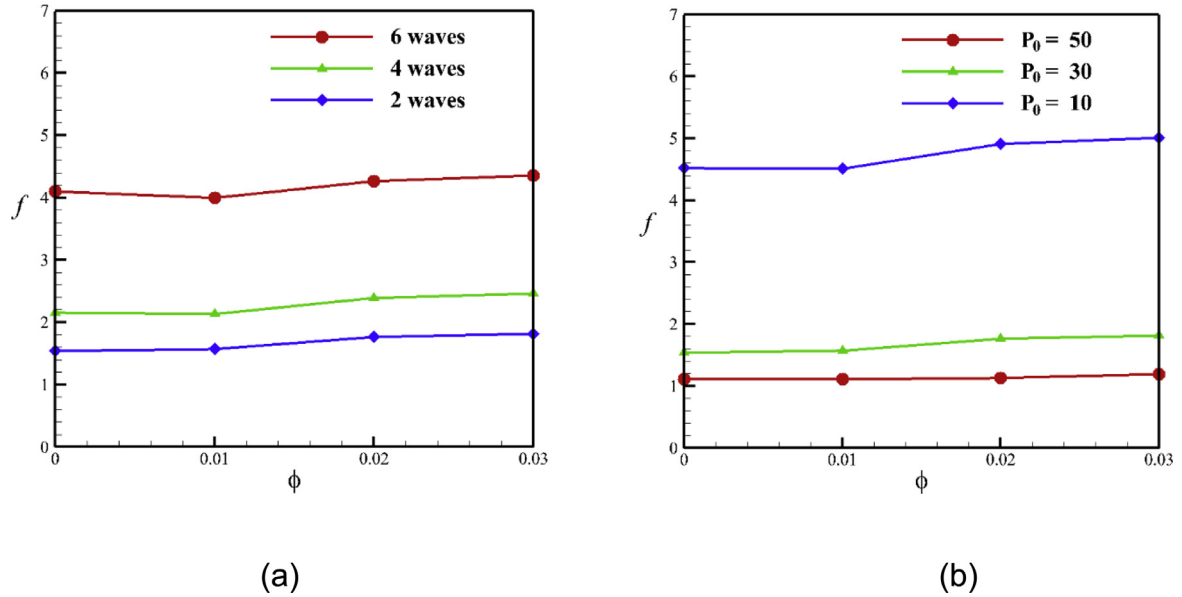

Fig. 12. Friction factor for wavy U-turn channel as a function of nanoparticle volume fraction with (a) various number of waves for $P_0 = 30$ and (b) different pressure gradients at $n = 2$.

in the wavy channel [17]. Fig. 9 shows non-dimensional isotherm lines for pure fluid (i.e. $\varphi = 0\%$) and nanofluid with $\varphi = 3\%$ for $P_0 = 50$. As shown in this figure, the thermal boundary layer thickness for nanofluid is smaller than that of the pure fluid in the wavy channel particularly on the trough of lower wall. Hence, the addition of nanoparticle causes a decrease in thermal boundary layer that consequently results in promotion in temperature gradients and Nu number at the wavy walls.

Fig. 10 shows the averaged Nu number, Nu_{ave}, along the wavy U-turn channel with $n = 4$ and 6 at $P_0 = 50$. It can be seen that Nu_{ave} first experiences a quite sudden and sharp decrease and then experiences increasingly larger variations with the minimum and maximum values corresponding to the crest and trough of the channel, respectively. As it is showed earlier when the fluid flowing in such channels, the reversal flow occurs in trough (crest) of lower (upper) wall. The reversal flow becomes pronounced as the pressure gradient or number of waves increases (see Figs. 5 to 8). The maximum and minimum values of Nu_{ave} occurs upstream and downstream within a short distance of the trough of each wave. This is because the former has higher temperature gradients than the latter and hence a higher heat transfer rate at this location.

Fig. 11 reveals the average Nu in various nanoparticle volume fractions, φ, at different number of waves in Fig. 11(a), and various pressure gradient in Fig. 11(b). As it is expected the variations in Nu_{ave} undergo increasingly larger changes as the volume fraction of nanoparticles increases. However this increment is more significant at higher pressure gradient ($P_0 = 50$) as it can be seen in Fig. 11(b). The average Nu is a decreasing function of number of waves, because of by making more waves along the channel with constant pressure gradient, friction factor

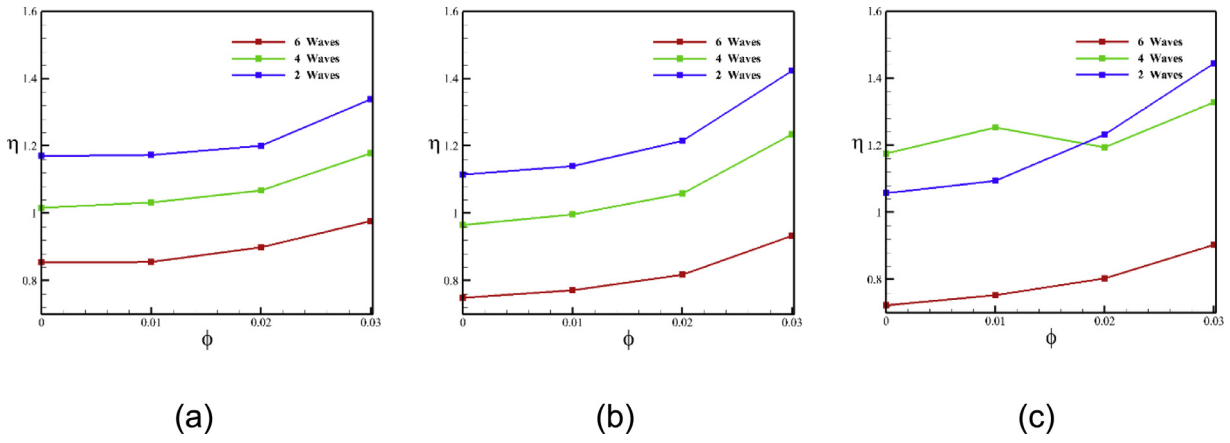

Fig. 13. Performance factor for wavy U-turn channel as a function of nanoparticle volume fraction with various number of waves for (a) $P_0 = 10$, (b) $P_0 = 30$ and (c) $P_0 = 50$.

dramatically rises (see Figs. 12(a)) and lead to lower fluid velocity in the channel. Consequently heat transfer rate decreases by dropping *Re* number. On the other hand, the friction factor has an inverse relation with Reynolds number. Thus by increasing pressure gradient, when the Re number rises in the channel, the friction factor decreases sharply as can be seen in Fig. 12(b).

In order to quantify the overall thermal performance and pressure drop on the U-turn wavy channel when the Al_2O_3-water nanofluid flows, the thermal–hydraulic performance factor, η, as a function of nanoparticle volume fraction, φ, and for various number of waves and P_0 are shown in Fig. 13. It can be explicitly observed that the performance factor increases with an increase in the nanoparticles volume fraction due to improved thermal conductivity of the base fluid. It is worth mentioning that the friction factor nanofluids, which is appeared in the denominator of the performance factor (see Eq. (35)), increases with increasing nanoparticle volume fraction at the constant P_0, but the growth of Nu number is more than friction factor. Consequently, by increasing Nu number and friction factor at the presence of nanofluids the performance factor enhances at the channel.

The performance factor shows significant dependence on number of waves, n. It can be seen that for small P_0 (i.e. 10 and 30, see Figs. 13(a) and 13(b)), the performance factor decreases by increasing the number of waves in the channel. The reason is that the friction factor significantly increases as the number of waves in the channel rises while the Nu number increases with lower rate thus leading to a decrease in η. However, for larger pressure gradients (i.e. $P_0 = 50$), the performance factor for $n = 4$ becomes slightly larger than the case with $n = 2$ which is due to the formation of recirculating regions in the channel leading to better heat transfer in the channel which cause a change in the trend of η in larger pressure gradients.

For the steady flow which we have studied here, it can be concluded that even though the wavy walled channels with large number of waves enhances heat transfer at the constant Re number, the increased friction factors associated with the geometry can lead to lower performance factor than that of channels with smaller n or flat channels.

5. Conclusion

In this paper, force convection heat transfer of Al_2O_3-water nanofluid through a wavy U-turn channel was investigated numerically using the thermal LBM approach. The effect of dimensionless pressure gradient, number of waves along the channel and nanoparticle volume fraction on the thermo-hydrodynamics of flow were examined. It was found that by increasing the pressure gradient (number of waves in the channel), the rate of heat transfer increases (decreases). Also the results showed that the thermal–hydraulic performance factor grows by increasing nanoparticles volume fraction at the same pressure gradient. Validation of present numerical results with previous published data available in the literature demonstrates that the LBM is a reliable and accurate approach for predicting the correct behavior for thermal flows in complex geometries.

References

[1] Levenspiel O. Chemical reaction engineering. Ind Eng Chem Res 1999;38(11):4140–3.
[2] Weilin Q, Mudawar I. Flow boiling heat transfer in two-phase micro-channel heat sinks-I. Experimental investigation and assessment of correlation methods. Int J Heat Mass Trans 2003;46(15):2755–71.
[3] Selimefendigil F, Öztop HF. Mixed convection of nanofluids in a three dimensional cavity with two adiabatic inner rotating cylinders. Int J Heat Mass Tran 2018;117:331–43.
[4] Selimefendigil F, Öztop HF. Jet impingement cooling and optimization study for a partly curved isothermal surface with CuO-water nanofluid. Int Commun Heat Mass 2017;89:211–18.
[5] Pinto RV, Fiorelli FAS. Review of the mechanisms responsible for heat transfer enhancement using nanofluids. Appl Therm Eng 2016;108:720–39.
[6] Zarghami A, Ubertini S, Succi S. Finite-volume lattice Boltzmann modeling of thermal transport in nanofluids. Comput Fluids 2013;77:56–65.
[7] Selimefendigil F, Öztop HF. Modeling and optimization of MHD mixed convection in a lid-driven trapezoidal cavity filled with alumina–water nanofluid: Effects of electrical conductivity models. Int J Mech Sci 2018;136:264–78.
[8] Sheikholeslami M, Ganji DD. Numerical modeling of magnetohydrodynamic CuO—Water transportation inside a porous cavity considering shape factor effect. Colloid Surface A 2017;529:705–14.
[9] Wang L, Sundén B, Manglik RM. Plate heat Exchangers: Design, applications and performance. Boston: WIT Press; 2007.
[10] Min J, Webb RL. Numerical predications of wavy fin coil performance. J Enhanc Heat Transf 2001;8(3):159–73.
[11] Metwally HM, Manglik RM. Enhanced heat transfer due to curvature induced lateral vortices in laminar flows in sinusoidal corrugated-plate channels. Int. J. Heat Mass Tran 2004;47(10–11):2283–92.
[12] Sui Y, Teo CJ, Lee PS. Direct numerical simulation of fluid flow and heat transfer in periodic wavy channels with rectangular cross-sections. Int. J. Heat Mass Tran 2012;55(1–3):73–88.
[13] Mohamed N, Wided BR, Mohamed E, Abd el Karim M, Mohamed B. Numerical investigation on the fluid flow and heat transfer in the entrance region of wavy channel. Energy Proc 2013;36:76–85.
[14] Rashidi MM, Hosseini A, Pop I, Kumar S, Freidoonimehr N. Comparative numerical study of single and two-phase models of nanofluid heat transfer in wavy channel. Appl Math Mech 2014;35(7):831–48.
[15] Mills ZG, Warey A, Alexeev A. Heat transfer enhancement and thermal–hydraulic performance in laminar flows through asymmetric wavy walled channels. Int J Heat Mass Tran 2016;97:450–60.
[16] Nishimura T, Kajimoto Y, Kawamura Y. Mass-transfer enhancement in channels with a wavy wall. J Chem Eng Jpn 1986;19(2):142–4.
[17] Ahmed MA, Yusoff MZ, Ng KC, Shuaib NH. The effects of wavy-wall phase shift on thermal–hydraulic performance of Al2O3–water nanofluid flow in sinusoidal wavy channel. Case Stud Therm Eng 2014;4:153–65.
[18] Nishimura T. Oscillatory flow and mass-transfer within asymmetric and symmetrical channels with sinusoidal wavy walls. Heat Mass Transf 1995;30(4):269–78.
[19] Ahmed MA, Shuai NH, Yusoff MZ. Numerical investigations on the heat transfer enhancement in a wavy channel using nanofluid. Int J Heat Mass Tranf 2012;55:5891–8.

[20] Yang YT, Wang YH, Tseng PK. Numerical optimization of heat transfer enhancement in a wavy channel using nanofluids. Int Commun Heat Mass 2014;51:9–17.
[21] Heidary H, Kermani MJ. Effect of nano-particles on forced convection in sinusoidal-wall channel. Int Commun Heat Mass 2010;37:1520–7.
[22] Akbarzadeh M, Rashidi S, Bovand M, Ellahi R. A sensitivity analysis on thermal and pumping power for the flow of nanofluid inside a wavy channel. J Mol Liq 2016;220:1–13.
[23] Esfahani JA, Akbarzadeh M, Rashidi S, Rosen MA, Ellahi R. Influences of wavy wall and nanoparticles on entropy generation over heat exchanger plat. Int J Heat Mass Tranf 2017;109:1162–71.
[24] Hasanpour A, Farhadi M, Sedighi K, Ashorynejad HR. Numerical study of Prandtl effect on MHD flow at a lid-driven porous cavity. Int J Numer Meth Fl 2012;70:886–98.
[25] Ashorynejad HR, Mohamad AA, Sheikholeslami M. Magnetic field effects on natural convection flow of a nanofluid in a horizontal cylindrical annulus using lattice Boltzmann method. Int J Therm Sci 2013;64:240–50.
[26] Zarghami A, Padding JT. Drag, lift and torque acting on a two-dimensional non–spherical particle near a wall. Adv Powder Technol 2018;29(6):1507–17.
[27] Hussein AK, Ashorynejad HR, Sheikholeslami M, Sivasankaran S. Lattice Boltzmann simulation of natural convection heat transfer in an open enclosure filled with Cu–water nanofluid in a presence of magnetic field. Nucl Eng Des 2014;268:10–17.
[28] Mukherjee S, Zarghami A, Haringa C, van As K, Kenjereš S, Van den Akker HEA. Simulating liquid droplets: a quantitative assessment of lattice Boltzmann and volume of Fluid methods. Int J Heat Fluid Fl 2018;70:59–78.
[29] Kefayati GHR. Mixed convection of non-Newtonian nanofluid in an enclosure using Buongiorno's mathematical model. Int J Heat Mass Tranf 2017;108:1481–500.
[30] Ashorynejad HR, Shahriari A. MHD natural convection of hybrid nanofluid in an open wavy cavity. Results Phys 2018;9:440–55.
[31] Sheikholeslami M, Ganji DD, Moradi R. Forced convection in existence of Lorentz forces in a porous cavity with hot circular obstacle using nanofluid via Lattice Boltzmann method. J Mol Liq 2017;246:103–11.
[32] Hoseinpour B, Ashorynejad HR, Javaherdeh K. Entropy generation of nanofluid in a porous cavity by lattice Boltzmann method. J Thermophys Heat Transf 2017;31:20–7.
[33] Ashorynejad HR, Hoseinpour B. Investigation of different nanofluids effect on entropy generation on natural convection in a porous cavity. Eur J Mech B-Fluid 2017;62:86–93.
[34] Succi S. The lattice boltzmann equation for fluid dynamics and beyond. Oxford Univ. Press; 2001.
[35] Sheikholeslami M. Lattice Boltzmann method simulation for MHD non-Darcy nano fluid free convection. Physica B 2017;516:55–71.
[36] Lai FH, Yang YT. Lattice Boltzmann simulation of natural convection heat transfer of Al2O3/water nanofluids in a square enclosure. Int J Therm Sci 2011;50(10):1930–41.
[37] Kefayati GHR, Tang H. Simulation of natural convection and entropy generation of MHD non-Newtonian nanofluid in a cavity using Buongiorno's mathematical model. Int J Hydrogen Energy 2017;42(27):17284–327.
[38] Ashorynejad HR, Zarghami A. Magnetohydrodynamics flow and heat transfer of Cu-water nanofluid through a partially porous wavy channel. Int J Heat Mass Transf 2018;119:247–58.
[39] Keith TG, Papa F, Dewitt KJ, Vaidyanathan K. Numerical calculation of developing laminar flow in rotating ducts with a 180° bend. Int J Numer Method Heat Fluid Flow 2002;12(7):780–99.
[40] Kardani A, Omidvar P, Zarghami A. Analysis of thermal flow in a rotating porous U-turn duct using lattice Boltzmann method. Transport Porous Med 2017;116(1):295–318.
[41] Zarghami A, Maghrebi MJ, Ghasemi J, Ubertini S. Lattice Boltzmann finite volume formulation with improved stability. Commun Comput Phys 2012;12(1):42–64.
[42] Guo Z, Zheng C, Shi B, Zhao TS. Thermal lattice Boltzmann equation for low Mach number flows: decoupling model. Phys Rev E 2007;75:036704.
[43] Zarghami A, Ubertini S, Succi S. Finite volume formulation of thermal lattice Boltzmann method. Int J Numer Method Heat Fluid Flow 2014;24(2):270–89.
[44] Zarghami A, Van den Akker HEA. Thermohydrodynamics of an evaporating droplet studied using a multiphase lattice Boltzmann method. Phys Rev E 2017;95(4):043310.
[45] Sheikholeslami M, Ashorynejad HR, Rana P. Lattice Boltzmann simulation of nanofluid heat transfer enhancement and entropy generation. J Mol Liq 2016;214:86–95.
[46] Abu-Nada E. Effects of variable viscosity and thermal conductivity of Al2O3–water nanofluid on heat transfer enhancement in natural convection. Int J Heat Fluid Flow 2009;30(4):679–90.
[47] Patel HE, Sundararajan T, Das SK. A cell model approach for thermal conductivity of nanofluids. J. Nanopart Res 2008;10:87–97.
[48] McCutcheon SC, Martin JL, Barnwell TO. Handbook of hydrology. New York: McGraw-Hill; 1993.
[49] Sherman FC. Viscous flow. New York: McGraw-Hill; 1990.
[50] Bergman TL, Lavine AS, Incropera FP, Dewitt DP. Fundamentals of heat and mass transfer. John Willey & Sons; 2011.
[51] Zou Q, He X. On pressure and velocity boundary conditions for the lattice Boltzmann BGK model. Phys Fluids 1997;9:1591–8.
[52] Ashorynejad HR, Javaherdeh K, Van den Akker HEA. The effect of pulsating pressure on the performance of a PEM fuel cell with a wavy cathode surface. Int J Hydrogen Energy 2016;41(32):14239–51.
[53] Mei R, Luo L-S, Shyy W. An accurate curved boundary treatment in the lattice Boltzmann method. J Comput Phys 1999;155:307–30.
[54] Mei R, Yu D, Shyy W, Luo L-S. Force evaluation in the lattice Boltzmann method involving curved geometry. Phys Rev E 2002;65(4):041203.
[55] Bouzidi M, Firdaouss M, Lallemand P. Momentum transfer of a lattice-Boltzmann fluid with boundaries. Phys Fluids 2002;13:3452–9.
[56] Mohamad AA. Applied lattice Boltzmann method for transport phenomena. Momentum, heat and mass transfer. Calgary, Canada: Sure Print; 2007.
[57] Orlanski I. A simple boundary condition for unbounded hyperbolic flows. J Comput Phys 1976;21:251–69.
[58] Guo Z, Zheng C, Shi B. An extrapolation method for boundary conditions in lattice Boltzmann method. Phys Fluids 2002;14(6):2007–10.
[59] Ahmed M, Yusoff M, Ng K, Shuaib N. The effects of wavy-wall phase shift on thermal–hydraulic performance of Al2O3–water nanofluid flow in sinusoidal wavy channel, Case Stud. Therm. Eng. 2014;4:153–65.
[60] Wang CC, Chen CK. Forced convection in a wavy-wall channel. Int J Heat Mass Transf 2002;45(12):2587–95.
[61] Rush TA, Newell TA, Jacobi AM. An experimental study of flow and heat transfer in sinusoidal wavy passages. Int J Heat Mass Transf 1999;42:1541–53.